ELSEVIER

Journal of Power Sources 85 (2000) 284–293

JOURNAL OF POWER SOURCES

www.elsevier.com/locate/jpowsour

Preparation of spinel lithium manganese oxide by aqueous co-precipitation

A.R. Naghash, Jim Y. Lee *

Department of Chemical and Environmental Engineering, National University of Singapore, 10 Kent Ridge Crescent, Singapore 119260, Singapore

Received 12 July 1999; accepted 5 August 1999

Abstract

Stearic acid in tetramethylammonium hydroxide is used to co-precipitate lithium and manganese in stoichiometric proportions from aqueous solutions of manganese and lithium salts. Calcination of the precipitate in air produces uniformly sized, fine particles of spinel $LiMn_2O_4$ as the end product. The effect of heat treatment on the spinel formation reaction is followed by thermogravimetry and powder X-ray diffraction measurements. The electrochemical performance of the spinel is evaluated in test cells using the spinel as the positive electrode material, and lithium metal as the negative electrode. The charge–discharge data indicate that the spinel has a specific capacity of about 119 mAh g^{-1}. The material shows good rate capability in the range of 0.5–3 mA cm^{-2}.

Keywords: Lithium-ion batteries; Lithium manganese oxide; Co-precipitation; Spinel; Cathode

1. Introduction

Layered ($LiCoO_2$ or $LiNiO_2$) or spinel ($LiMn_2O_4$) oxides are known to intercalate lithium ions reversibly at potentials greater than 3.5 V (vs. Li). Thus, secondary batteries using these materials as the positive electrode have high cell voltages and specific energies [1]. The cells are assembled in the discharged state and can be stored for an extended period without degradation.

Among these materials, $LiMn_2O_4$ is most noted for being environmentally benign and can be offered at a lower cost [2–4]. Although the theoretical capacity of $LiMn_2O_4$ (148 mAh g^{-1}) is lower than that of either $LiCoO_2$ or $LiNiO_2$, its utilization is higher and a reversible capacity of 120 mAh g^{-1}, or 80% of the theoretical capacity can often be realized in most of the 4-V designs of battery.

Spinel $LiMn_2O_4$ is usually synthesized at high temperatures (700°C to 800°C) by solid-state reactions [5]. At lower temperatures, some Mn_2O_3 may be present as an impurity which only disappears at 800°C [6–8]. The use of MnO_2 as a starting material was reported [9,10] to lower the synthesis temperature to 700°C and below. Soft chemistry methods, such as sol–gel processes, have been able to reduce further the heat-treatment temperature because the starting material is mixed more intimately and this reduces the barrier against mutual ion diffusion at the synthesis temperature [11–16]. An added advantage of low temperature synthesis is that smaller particles can be produced which allows better material utilization in high-rate applications. Co-precipitation synthesis of $LiMn_2O_4$ precursors is an attractive alternative, but is often hindered by the high solubility of lithium salts in water, and attaining good stoichiometric control of the Li:Mn ratio in the end product is the greatest challenge. Recently, Qiu et al. [17] have successfully carried out co-precipitation from non-aqueous solutions.

We report here a co-precipitation procedure which can be carried out in water using an organic precursor such as stearic acid. This method allows a more intimate mixing of lithium and manganese in the starting materials which results in a homogeneous $LiMn_2O_4$ product with well-controlled morphology. $LiMn_2O_4$ prepared as such was characterized by thermogravimetry (TG), differential thermogravimetry (DTG), differential thermal analysis (DTA), X-ray diffraction (XRD), inductive coupling plasma (ICP) spectroscopy, and scanning electron microscopy (SEM).

* Corresponding author. Tel.: +65-874-2899; fax: +65-779-1936; e-mail: cheleejy@nus.edu.sg

0378-7753/00/$ - see front matter
PII: S0378-7753(99)00347-X

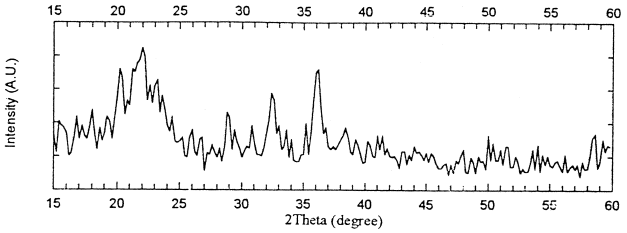

Fig. 1. XRD pattern of co-precipitated oxide precursor.

Electrochemical data were obtained from test cells using lithium metal as the counter electrode.

2. Experimental

2.1. Material preparation

Stearic acid (BDH), $MnSO_4$ (Merck 99%), Li_2CO_3 (Fisher), $LiNO_3$ (Sigma, 99%), $MnCO_3$ (Merck), and tetramethylammonium hydroxide (Merck) were of the purest grade commercially available and were used as received. Some $LiMn_2O_4$ was prepared by solid state reactions for comparison. In such cases, $LiCO_3$ and $MnCO_3$ were mixed in a mole ratio of 1:4 in a blender. The mixed powder was pelletized and calcined in air at 800°C for 24 h. By contrast, synthesis by co-precipitation was carried out by mixing aqueous solutions of $LiNO_3$ and $MnSO_4$ in amounts which correspond to the final stoichiometry of $LiMn_2O_4$. The mixture was then added drop-wise under a nitrogen atmosphere to a stirred solution of stearic acid (in equimolar quantity to $LiNO_3$) in tetramethylammonium hydroxide (TMAH). The pH was kept between 8 and 10 by using acetic acid. The precipitate formed was aged in situ for 1 h before it was removed by filtration, washed, and dried in an vacuum oven at 80°C overnight. It was subsequently ground into fine powder and calcined in flowing air at different temperatures for different lengths of time at a rate of 1°C min^{-1}.

2.2. Material characterizations

TG, DTG and DTA were carried out on a Netzsch STA 409 analyzer, using 10 mg of the co-precipitate, 100 ml min^{-1} of flowing air, and a heating rate of 5°C min^{-1} in the temperature range of 20°C–1000°C. XRD analyses of $LiMn_2O_4$ and various intermediate oxides were carried out on a Philips PW 1877 automated powder diffractometer using monochromated Cu K_α ($\lambda = 1.542$) radiation. A Micromeritics Flowsorb II 2300 was used for the measurement of BET surface area. Chemical analysis by ICP was carried out using a Perkin Elmer Optima 3000 instrument and digestion of $LiMn_2O_4$ in aqua regia. The morphology of $LiMn_2O_4$ was examined with a JEOL JSM-T330A scanning electron microscope.

2.3. Electrochemical characterization

Electrochemical characterization of $LiMn_2O_4$ was carried out in two-electrode test cells with metallic lithium counter electrodes. A commercial (Merck) 1 M $LiPF_6$ solution in a 1:1 EC/DMC mixture was used as the electrolyte. The positive electrode was constituted from 85% $LiMn_2O_4$, 10% carbon black, and 5% PVDF. The electrode mix was pasted on to aluminum foil and compressed at a pressure of 2 t cm^{-2}. The cathode material loading was between 6 and 8 mg cm^{-2}.

3. Results and discussion

3.1. Composition of co-precipitated precursor

The XRD pattern of the solid precursor after filtration and drying in a vacuum oven is shown in Fig. 1. The peak positions are also listed in Table 1 alongside the XRD peaks of lithium stearate (JCPDS 04-0352) and Mn(II) hydroxide (pyrochrote, JCPDS 12-0696) for comparative identification. It is obvious that the precursor is a physical mixture of lithium stearate and manganese hydroxide. ICP analysis of $LiMn_2O_4$ obtained by heating the precursor showed a Li:Mn mole ratio of around 0.49:1. This indicates good stoichiometry control of the spinel composition by this alternative method of preparation.

3.2. Thermogravimetric analysis of the co-precipitated precursor

TG–DTG–DTA traces of the decomposition of pure lithium stearate in air are presented in Fig. 2(a). The TG response can be broadly divided into two regions: (i) an initial weight loss of 14% between 200°C and 410°C, (ii) a further weight loss of 70.5% that is nearly complete around 520°C.

Table 1
XRD peak positions (in 2θ)

	2θ value												
Lithium stearate		21.0	21.6	22.4	23.8	25.5	28.9	32.8	36.5	38.3	50.2	54.3	56.2
$Mn(OH)_2$	18.8							32.2	36.6	38.1		54.4	
Fig. 1	19.0	20.5	21.2	22.1	23.5	25.5	28.8	32.0	36.1	38.3	50.0	54.0	56.2

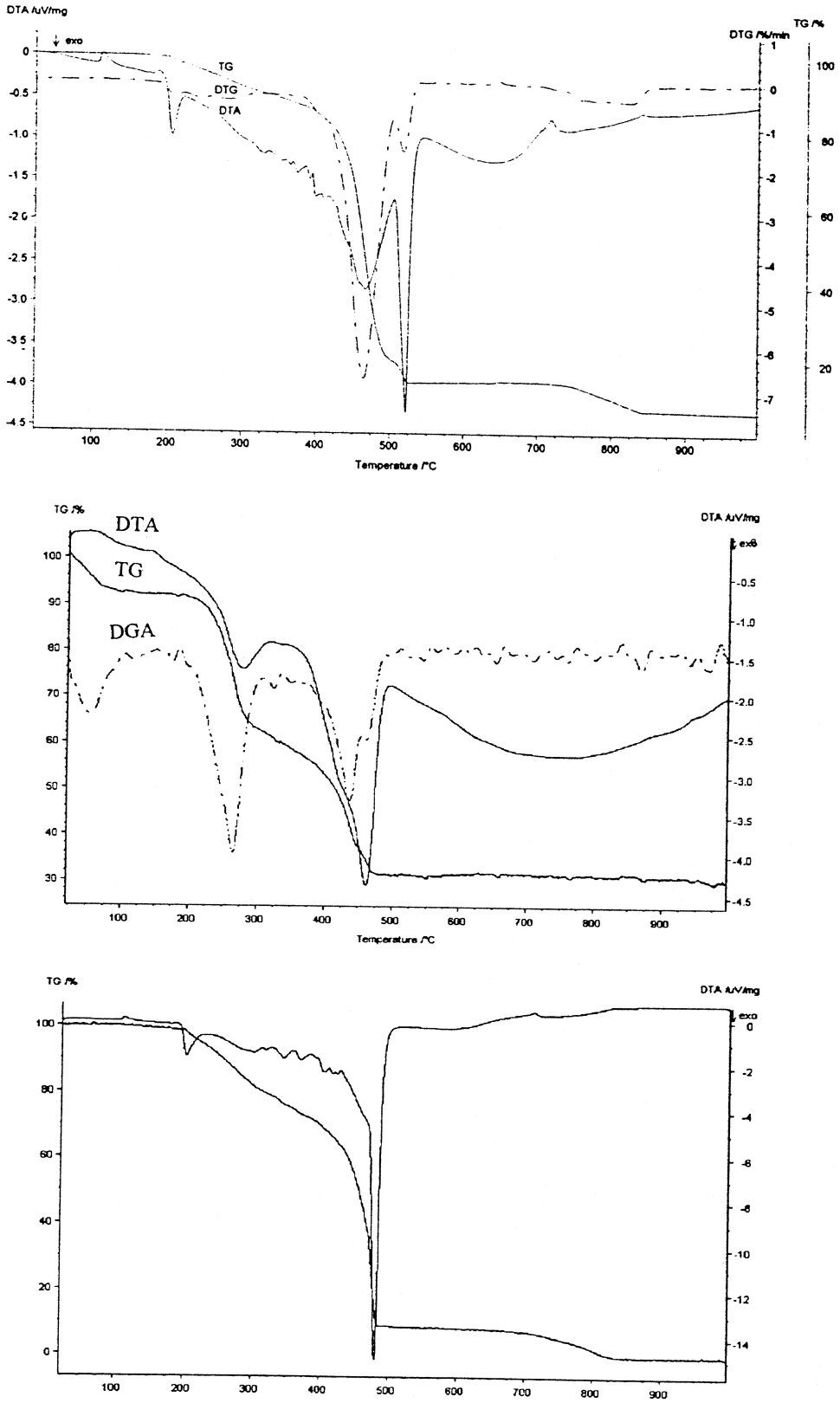

Fig. 2. TG–DTA traces of: (a) lithium stearate in flowing air; (b) co-precipitated oxide precursor heated to 1000°C at 5°C min^{-1} in flowing air; (c) lithium stearate in flowing oxygen.

The TGA–DTG–DTA curves of the dry co-precipitated precursor are shown in Fig. 2(b). The small DTG peak below 100°C, which accounts for 7% of the initial weight loss in TG and corresponds to the endothermic peak in

DTA, is assigned to the loss of free water. The weight loss thereafter can be divided into two temperature regions, namely, from 200 to 340°C, and from 340°C to 500°C, which correspond to further weight losses of 33% and 28%, respectively. The large DTA peak in the second temperature region can be contributed by two superimposed exothermic processes. Comparison of Fig. 2(a) and (b) shows that the rate of temperature rise for lithium stearate decomposition is lower in the presence of manganese hydroxide. This suggests that the decomposition of the latter is facilitated by the large amount of exothermic heat which generated in the decomposition of lithium stearate.

The decomposition of pure lithium stearate in oxygen was also followed by TGA–DTA (Fig. 2(c)). The first thermal effect culminated in a weight loss of 40%, a value much higher than that for decomposition in air. The large exothermic peak in the DTA data is caused by the highly exothermic nature of stearate decomposition in oxygen (the maximum DTA peak is 14 μV for oxygen and 4 μV for air). Such heat effects may cause ''hot spots'' to develop in the powder bed that lead to the sintering of particles [16]. From these results, it can be deduced that better powder morphology may be obtained by heating in air instead of oxygen.

3.3. Structural characterization

The co-precipitated precursor was heated to different temperatures and its evolution to a final spinel structure was closely monitored by powder XRD. The pattern of the precursor after heating at 250°C for 2 h is shown in Fig. 3(a). The intensity reduction for peaks between 2θ of 20° and 27° is consequential upon lithium stearate decomposition around 200°C. The decomposition was not complete as a major peak at 36.12° and satellite peaks at 38.31°,

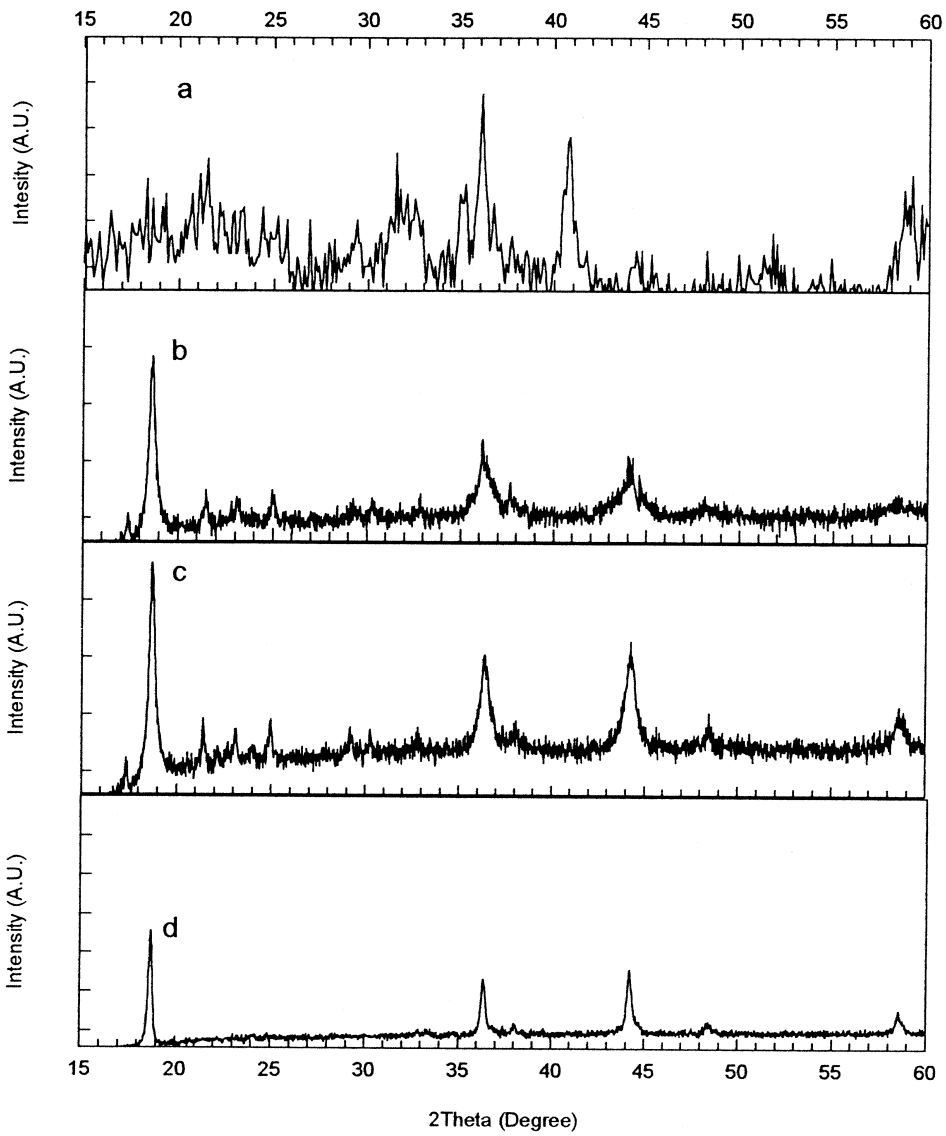

Fig. 3. XRD patterns of co-precipitated oxide precursors heat treated at: (a) 250°C for 2 h; (b) 250°C for 100 h; (c) 400°C for 48 h; (d) 650°C for 48 h.

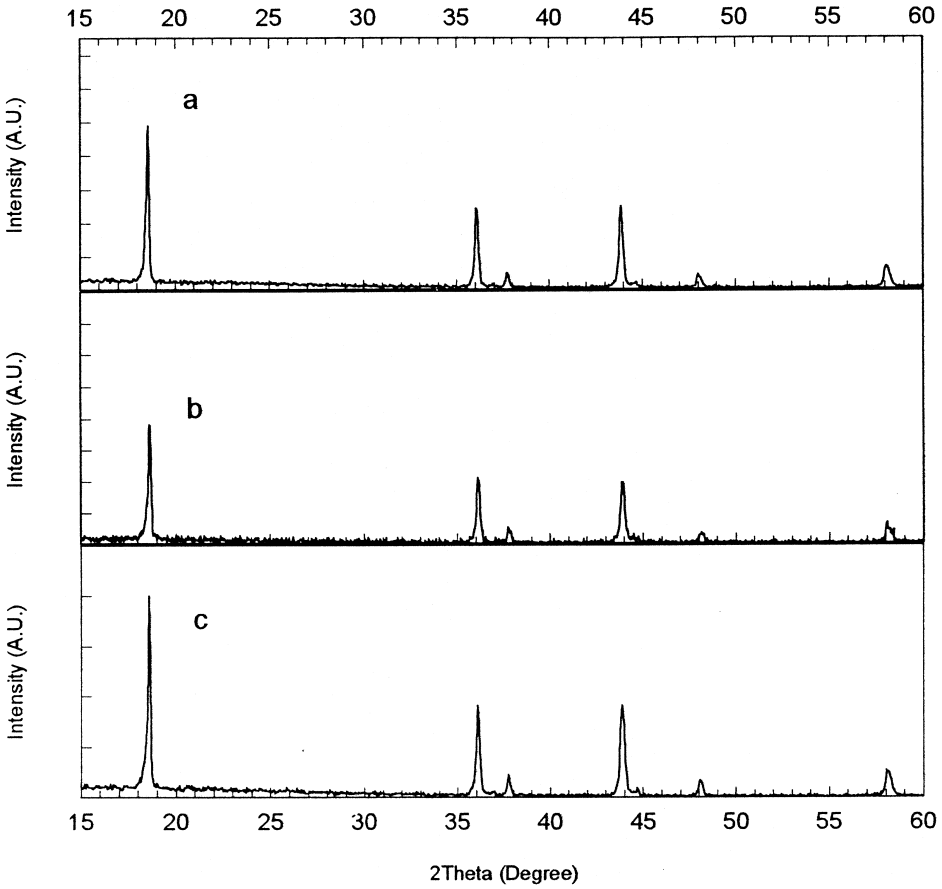

Fig. 4. XRD patterns of co-precipitated oxide precursors heat treated at: (a) 850°C for 3 h; (b) 850°C for 12 h; (c) 850°C for 18 h.

44.35°, 50.98° and 53.98° — all characteristic of remnant lithium stearate structure — are still evident. These observations are consistent with the TG findings that the decomposition progresses in two stages (200°C to 340°C, and 340°C to 500°C, with more weight loss in the second stage). Four additional peaks at 2θ of 32°, 36.1°, 40.5° and

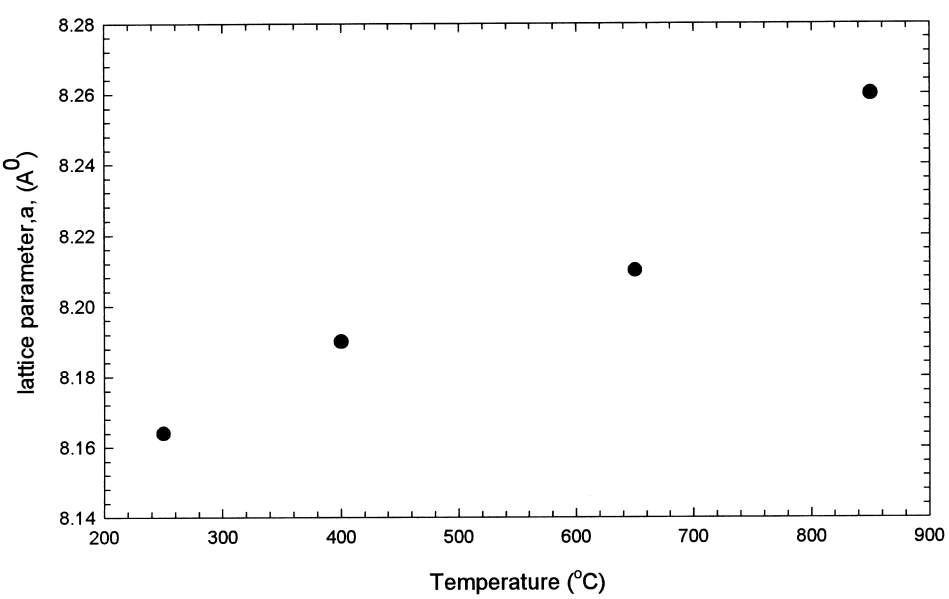

Fig. 5. Lattice parameter a vs. heating temperature for spinels prepared at different temperature.

59°, which were absent in Fig. 1, were also found. These peaks could be satisfactorily indexed with respect to the four most prominent peaks of MnO (JCPDS 07-0230, 31.6° (60), 36° (100), 40.54° (60), 58.72° (60)). It can therefore be deduced that at this early stage of heating, the stearate has partially decomposed to smaller hydrocarbon fragments, and $Mn(OH)_2$ has decomposed to MnO.

The XRD pattern of a precursor after firing at 250°C for 100 h is given in Fig. 3(b). It is obvious that the basic structure of $LiMn_2O_4$ can be formed after prolonged heating at this relatively low temperature. The material is, however, not phase-pure as there are additional peaks in the XRD that do not belong to the spinel phase. These peaks could have resulted from residual sulfates in the starting materials that require higher temperatures for their removal. The XRD pattern also shows broader peaks at high scattering angles.

The powder XRD pattern obtained from a precursor after firing at 400°C for 48 h is presented in Fig. 3(c). The pattern is almost the same as that in Fig. 3(b) except that the peak widths are narrower and there is less peak broadening at high 2θ values. The XRD pattern of a precursor heat treated at 650°C for 48 h is shown in Fig. 3(d). The sharp diffraction peaks and the lack of spurious features indicate a phase-pure spinel structure with good crystallinity.

To investigate further the effect of heating on the formation of spinel $LiMn_2O_4$, the temperature was increased to 850°C for different lengths of time, as shown in Fig. 4. There is no change in the XRD pattern (e.g., peak

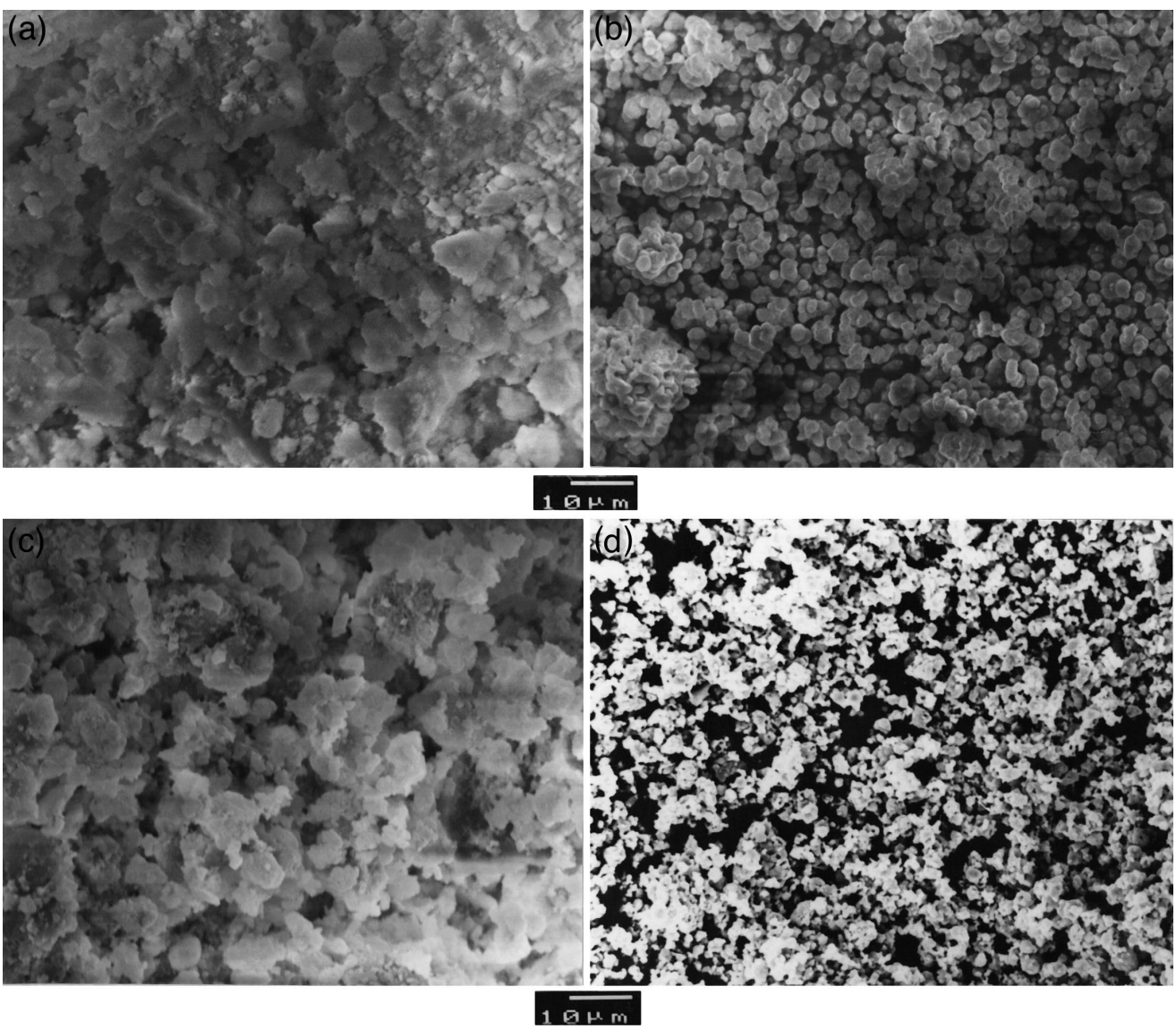

Fig. 6. Electron micrographs of: (a) co-precipitated oxide precursor; (b) mechanical mixture of Li and Mn carbonates; (c) $LiMn_2O_4$ prepared by co-precipitation; (d) $LiMn_2O_4$ prepared from mechanically mixed Li and Mn carbonates.

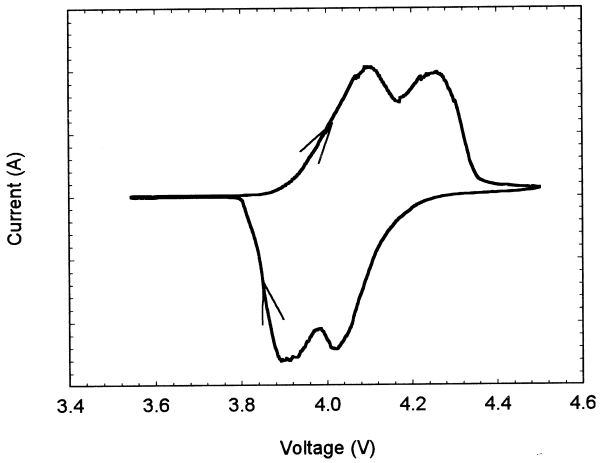

Fig. 7. Cyclic voltammogram of $LiMn_2O_4$ positive electrode between 3.5 and 4.5 V (vs. Li^+/Li) at 0.6 mV min^{-1}.

broadening) as the heating time is reduced from 18 to 3 h. It can therefore be concluded that temperature has an overriding influence over heating time, especially at higher temperatures.

The lattice parameter (a) of spinel $LiMn_2O_4$, obtained by indexing the XRD peaks using a least-squares program, is plotted against the heat-treatment temperature in Fig. 5. The lattice parameter increases with increasing temperature from 8.17 Å at 250°C for 100 h to 8.26 Å at 850°C. The increase in lattice parameter is an indication of the gradual formation of stoichiometric (defect-free) spinel. The lattice parameter also varies noticeably with heating temperature unless the spinel was fired at 850°C at different times (3, 12 and 18 h). The broadening of diffraction peaks at high scattering angles is indicative of the residual strains in the structure [14]. Residual strains are caused by inhomogeneities, cation or anion non-stoichiometry (vacancies), and grain boundary effects. The strains are only reduced through an increase in the heat-treatment temperature.

From the foregoing discussion, it is concluded that in the early stages of heating (250°C) the solution-based precursor decomposes without oxidation. Subsequent oxidation by oxygen is necessary to convert Mn^{2+} to a higher oxidation state in the final product. The progression of events can be summarized as follows:

Solution based precursor

$$\xrightarrow{250^\circ C} \text{decomposed product including } MnO + O_2$$

$$\xrightarrow{250^\circ C} \text{spinel phase}$$

$$\xrightarrow{\text{higher temperature}} \text{crystalline, single phase spinel.}$$

3.4. Particle size and surface area

The morphologies of the co-precipitated precursors and a mechanical mixture of lithium and manganese carbonates, as examined by SEM before any heat treatment, are shown in Fig. 6(a) and (b), respectively. Co-precipitation under the experimental conditions produces a very fine powder with a particle size which is much smaller than is possible with mechanically mixed carbonates. The corresponding morphologies of $LiMn_2O_4$ obtained from the precursor heat treated at 850°C for 3 h and mechanically mixed carbonates of lithium and manganese after calcination at 750°C for 48 h are shown in Fig. 6(c) and (d), respectively. The average particle size from these two methods are 2 and 8 μm, respectively. It should be emphasized that the powders were not ultrasonically treated prior to SEM examination. The $LiMn_2O_4$ derived from co-precipitation has a uniform distribution of particles in the micron range, whereas larger and more agglomerated particles with scattered size and shape distributions were formed from solid state reactions using mixed carbonates. From these comparisons, it can be deduced that the particle morphology of the final product is determined by the morphology of the starting materials. One of the most significant effects of small particle size is the ability to support higher rates of lithium intercalation and de-interca-

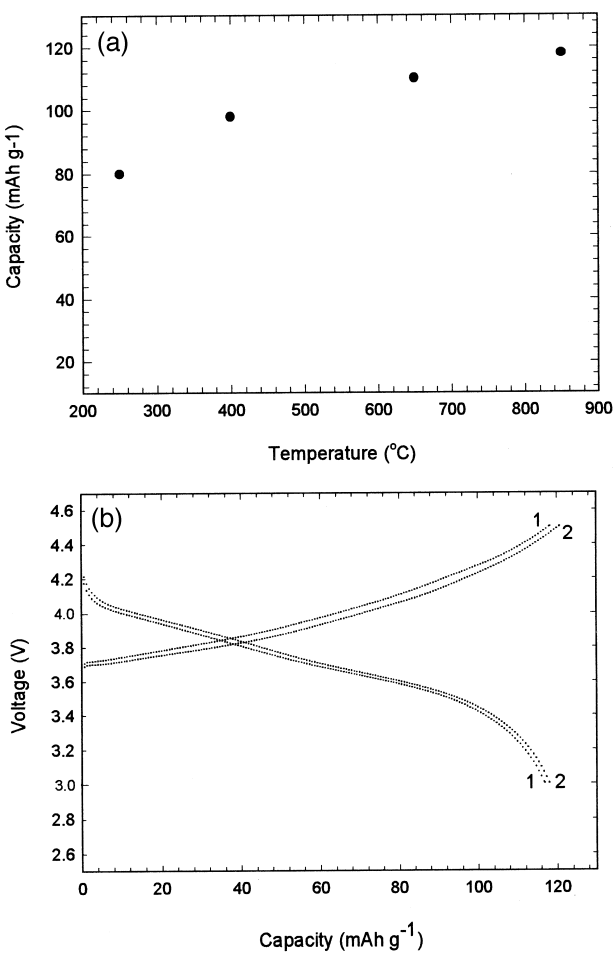

Fig. 8. (a) Initial discharge capacity for $LiMn_2O_4$ prepared from solution synthesis but fired at different temperature; (b) charge and discharge curves of $LiMn_2O_4$ prepared at 850°C for 3 h.

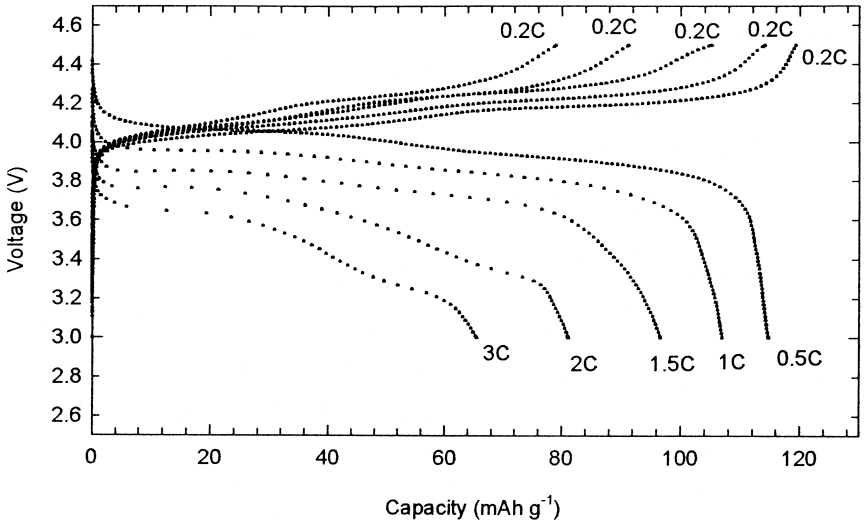

Fig. 9. Specific capacities of spinel heat treated at 850°C for 3 h at different current densities.

lation from the oxide host [3]. Both the current and power ratings of the material are expected to increase as a result.

4. Electrochemical analysis

4.1. Cyclic voltammetry

The voltammogram shown in Fig. 7 was obtained at a slow scan rate of 0.6 mV min^{-1}. Two oxidation peaks and two reduction peaks are found in the potential region between 3.5 to 4.5 V vs. Li^+/Li. These peaks are characteristic of a two-step reversible transformation between $LiMn_2O_4$ and λ-MnO_2 which results in lithium ion disordering during intercalation/de-intercalation. It is known that lithium ions shuttle between the electrolyte and the tetrahedral 8a sites of $LiMn_2O_4$ during charging and discharging. On discharging, the number of Li ions in the host structure increases and this, in turn, increases the interactions between each Li^+ and its four nearest Li^+ neighbours splits the oxidation peak [13]. Peak splitting is also observed for the reverse process of lithium extraction from the host.

4.2. Capacity

The average specific capacities from the first two cycles vs. the heating temperature are shown in Fig. 8. There is some levelling off in the increase in capacity with heat-treatment temperature after 650°C. A longer heating time at a low temperature may improve the capacity but such dependence is less evident at higher temperatures (the

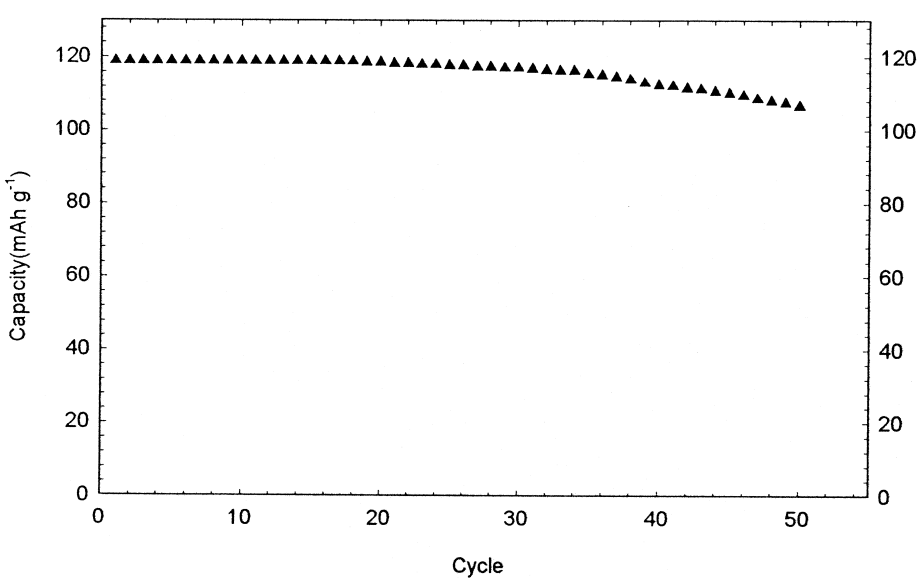

Fig. 10. Cycling performance of spinel prepared at 850°C for 3 h.

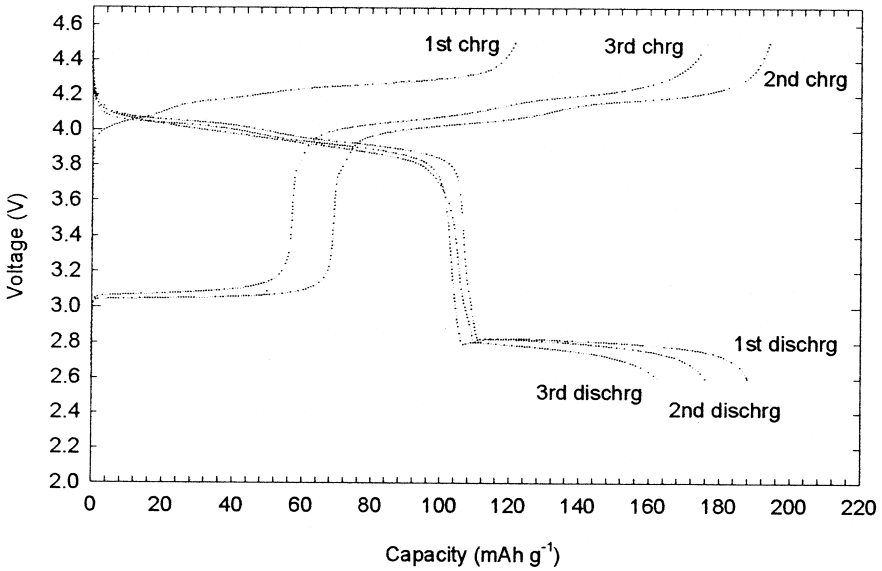

Fig. 11. First three charge–discharge curves between 2.6 and 4.5 V for spinel prepared at 850°C for 3 h.

capacities of spinel $LiMn_2O_4$ heat treated at 850°C for 12 and 18 h, respectively, deliver almost the same capacity). The charge–discharge curves for $LiMn_2O_4$ heat treated at 850°C for 3 h are presented in Fig. 8(b). The columbic efficiency is 96%. The slight increase in the second cycle performance is consequential upon cathode conditioning.

The electrochemical performance of an active battery material is dependent on its morphology (particle shape and size) and crystallinity. The smaller the particle size the lower is the true current density for a given overall current. This reduces most forms of polarization in the charge-transfer reaction between the intercalant and the intercalation host. The co-precipitation method described here is able to produce small particles of predominantly the spinel structure at temperature as low as 250°C. The spinel structure is refined in subsequent heat treatment without significant changes in the particle size. This retention of particle size is advantageous to the sustainability of high-rate capability. The specific capacity of the spinel heat treated at 850°C for 3 h at different current densities is shown in Fig. 9. At 0.5 and 1 mA cm^{-2}, capacities of 115 and 110 mAh g^{-1} were obtained, respectively, with corresponding mid-point discharge voltages of 4.05 and 3.95 V. The material displays good rate capability, even at a higher current density of 3 mA cm^{-2}, when compared with previous literature values [3]. The cyclability of the same material is shown in Fig. 10. This capacity fading of about 12% after 50 cycles is considerably good among un-optimized laboratory test cells and preparative procedures.

4.3. Suitability as a 3-V cathode material

Spinel $LiMn_2O_4$ can incorporate another lithium cation into its structure when it is discharged below 3 V. The insertion reaction is accompanied, however, by a change in the lattice structure from cubic to tetragonal that causes Jahn–Teller distortions and poor material reversibility in applications. A more tolerant material may be prepared through synthesis variations that yield different microstructure [3]. As a quick test, the co-precipitated spinel heat-treated at 850°C for 3 h was cycled between 2.6 and 4.5 V for three cycles (Fig. 11). The capacity fade of 11% for three cycles does not recommend operation below 3 V but the extent of the fade is considerably better than some of the previous attempts (30% loss after three cycles) [18,19].

For a uniform distribution of small particles, it is reasonable to assume that all particles have the same composition during discharge. When Jahn–Teller distortions occur, most particles will experience, to the same extent, the dimensional changes caused by a cubic to tetragonal phase transformation (the large anisotropic expansion of the unit cell results in a 16% increase in the c:a ratio of the cell parameters). This uniformity of change among all particles might help to retain the structural integrity between the particles, in particular the particle-to-particle contacts. The more tolerant nature of the co-precipitated spinel when subjected to sub-3 V cycling can be attributed to the more uniform distribution of smaller particles in this material.

5. Conclusions

Spinel $LiMn_2O_4$ was prepared by a co-precipitation method carried out in the aqueous phase. TGA, DTA and XRD analyses of the co-precipitated oxide precursor indicate an intimate mixture of lithium and manganese compounds that could be heated in air to form spinel $LiMn_2O_4$. Heat treatment under varying conditions show that $LiMn_2O_4$ can be formed at 250°C after extended heating, but higher temperature is required for good crystallinity of

the end product. The spinel formed by this method consists of uniform particles in the micron range. This is unattainable by solid-state reactions using mechanically mixed precursor salts of lithium and manganese. The voltammetric response typical of $LiMn_2O_4$ is obtained by cycling a $Li/EC + DMC, LiPF_6/LiMn_2O_4$ cell between 3.5 and 4.5 V at 0.6 mV min^{-1}. With an average specific capacity of 119 mAh g^{-1}, a good rate capability with current density in the range of 0.5–3 mA cm^{-2}, and a coulombic efficiency of 96%, the $LiMn_2O_4$ prepared by this method is suitable for lithium-ion battery applications.

Acknowledgements

The authors are grateful to Dr. J. Lin for his X-ray facility, Dr. Z.L. Liu for his assistance in cell assembly and testing, and Prof. K.G. Neoh for useful discussion on thermogravimetry.

References

[1] D. Guymard, J.M. Tarascan, J. Electrochem. Soc. 139 (1992) 937.
[2] M.M. Thacheray, J. Electrochem. Soc. 142 (1995) 2558.
[3] Z. Jiang, K.M. Abraham, J. Electrochem. Soc. 143 (1996) 1591.
[4] K. Amine, H. Tukamoto, H. Yasuda, Y. Fujila, J. Electrochem. Soc. 143 (1996) 1607.
[5] R.T. Cygan, H.R. Westrich, D.H. Doughty, Mater. Res. Symp. Proc. 393 (1995) 113.
[6] J.M. Tarascan, F. Coowar, G. Amatuci, F.K. Shokoohi, D.G. Guyomard, J. Power Sources 54 (1995) 103.
[7] R. Manev, A. Momchilv, A. Nassalevska, A. Sato, J. Power Sources 54 (1995) 323.
[8] Q. Zhong, U. Sachen, J. Power Sources 54 (1995) 221.
[9] R. Koksbang, J. Barker, H. Shi, M.Y. Saidi, Solid State Ionics 89 (1996) 1.
[10] T. Ohzuku, A. Ueda, N. Yamamoto, Y. Iwakoshi, J. Power Sources 54 (1995) 99.
[11] S. Maingot, Ph. Deniard, N. Baffier, J.P. Pereira-Ramos, A. Kahan-Harari, J. Power Sources 54 (1995) 342.
[12] J.M. Tarascon, E. Wang, F.K. Shokoohi, J. Electrochem. Soc. 138 (1991) 2859.
[13] P. Barboux, J.M. Tarascon, F.K. Shokoohi, Solid State Chem. 22 (1991) 185.
[14] A. Pathak, D.K. Mukhopadhyay, P. Pramanik, Mater. Res. Bull. 27 (1992) 155.
[15] G. Gusmano, P. Nunziante, E. Trarersa, G. Chiozzini, J. Therm. Anal. 37 (1991) 1697.
[16] J.A. Voigt, J.T. Boyle, D.H. Doughty, B.A. Hernandez, B.J. Johnson, S.C. Levy, C.J. Tafoya, M. Rosay, Mater. Soc. Symp. Proc. 393 (1995) 101.
[17] X. Qiu, X. Sun, W. Shen, N. Chen, Solid State Ionics 93 (1997) 335.
[18] M.M. Thackeray, A. de Kock, M.H. Rossouw, D.C. Liles, R. Bittihn, D. Hoge, J. Electrochem. Soc. 139 (1992) 363.
[19] W.J. Macklin, R.J. Neat, R.J. Powell, J. Power Sources (1991) 34.